CREEP OF CIRCULAR PLATES USING A STATE-VARIABLE APPROACH

Y.C. Waung and R.H. Lance

Department of Theoretical and Applied Mechanics
Cornell University
Ithaca, N.Y. 14853

ERDA Report #COO-2733-7

August 1976

DISCLAIMER

ABSTRACT

The technical theory of bending of circular plates under axisymmetric lateral loads is formulated in terms of Hart's state-variable equations. Then the method is applied to plates with simply supported and clamped edges through a standard algorithm. All the analytical results obtained compare qualitatively with those reported in the literature. The influence of the state variable called "hardness" is clearly demonstrated. Thus the analysis and the results provide a basis for acceptance of the model applied to structural components in a multiaxial state of stress.

INTRODUCTION

Due to the high temperature operating conditions of structural components used in the power generation industry and the aircraft industry, progress is needed in analysis and design incorporating the effect of creep [1]. Most of the engineering theories of creep are based on uniaxial-stress experimental data whereas components in service are usually in a multi-dimensional state of stress. Attempts at generalizing the creep theories within the framework of classical plasticity have been made [2].

One of the interesting cases is the creep-bending of thin circular plates. Malinin [3] analyzed the creep of symmetrically loaded plates using Galerkin's method. Using the maximum shearing stress criterion of plasticity, Venkatraman and Hodge [4] obtained the closed form solutions of plates under uniform lateral loads. Penny and Marriot [5], and Odqvist [6] presented general methods for obtaining the creep deflections of circular plates. A different approach involving simple analysis of moment equations was chosen by Patel, Cozzarelli and Venkatraman [7], and Patel [8]. Kachanov [9] introduced a variational principle to obtain solutions of plates under various loading conditions. Recently Sim [10] solved the problem of creep-bending of plates using the reference stress technique and compared analytical results with experiments. It must be emphasized that either a steady-state creep law or a time-hardening law was used in all the above analyses.

The classical creep theories with time, strain, etc., as variables do not take into account the effect of past history upon subsequent deformation and are incapable of representing creep recovery [11]. To represent creep behavior more closely, a state-variable theory due to Hart [12] has received much attention and tensile experiments to determine material parameters for

a wide class of metals have been carried out [13,14]. The theory was recently chosen for analysis of creep-bending of beams by the present authors [15], and for analysis of spheres and cylinders by Kumar and Mukherjee [16].

In this paper, first a general technical theory of bending of circular plates is formulated in terms of Hart's state-variable equations. It is felt that incorporation of a state variable, called "hardness", will account for the past history of loading in the material. It should be emphasized that "hardness" is a material parameter which can be determined experimentally [14]. The aim here is to develop, using the technical theory, solutions to classical problems in bending of circular plates which can be tested experimentally, and can be compared to the results of analysis using classical creep theories quoted before. Such comparisons may be useful in establishing a basis for this new model in a multiaxial state of stress.

Following the theoretical development, a simply supported circular plate under uniform lateral loads is analyzed. Numerical solutions for moment, stress and deflection are presented. The same approach is carried out for a clamped plate under the same loading condition.

As in the previous report [15], our study shows that results based on Hart's kinetic creep law generalized to a multiaxial state of stress through the concept of incremental plasticity and the notion of "hardness" are consistent with existing results; past history of loading has a strong influence on creep behavior.

FORMULATION OF A TECHNICAL PLATE THEORY

The basic problem of a plate undergoing creep is to determine its deflection as a function of time due to a suddenly imposed load which may subsequently vary with time. For engineering design purposes, it is equally essential to study other features of its mechanical behavior such as moment and stress distributions at various points of the plate.

For the sake of simplicity, the formulation is developed for a thin circular plate under axisymmetric loading as in Fig. 1. Let the radius of the plate be a and the thickness be h. The assumptions adopted in the technical plate theory are:

(i) the deflections w are small in comparison with the thickness h of the plate,

(ii) linear elements which are perpendicular to the central plane before strain remain linear elements perpendicular to the central surface after strain,

(iii) the central plane of the plate is not elongated; points in it are only displaced vertically,

(iv) the normal stresses and the direction transverse to the plate can be neglected, and

(v) loading is steady or slowly varying.

As creep is a time-dependent process, rate (evolution) equations must be formulated. We assume that the total strain rate tensor is the sum of an elastic strain rate tensor $\dot{e}_{ij}$ and a non-elastic strain rate tensor $\dot{e}^{n}_{ij}$, i.e.,

$$\dot{e}^{t}_{ij} = \dot{e}_{ij} + \dot{e}^{n}_{ij} \quad , \quad (\cdot) = \partial()/\partial t \tag{1}$$

Two separate creep strain rate components have been experimentally identified [17], i.e.,

$$\dot{e}^{n}_{ij} = \dot{e}^{a}_{ij} + \dot{p}_{ij} \tag{2}$$

where $\dot{e}^{a}_{ij}$ is the recoverable creep strain rate and $\dot{p}$ is the irrecoverable creep strain rate. If the loading is steady or slowly varying as assumed, e^{a}_{ij} will readily approach a saturation value e^{as}_{ij} and consequently its rate $\dot{e}^{a}_{ij} \approx 0$. Henceforth in the circular plate,

$$\dot{e}^{t}_{r} = \dot{e}_{r} + \dot{p}_{r} \quad \text{and} \quad \dot{e}^{t}_{\theta} = \dot{e}_{\theta} + \dot{p}_{\theta} \, . \tag{3}$$

From assumption (ii), it follows that

$$\dot{e}^{t}_{r} = y\dot{\kappa}_{r} \quad , \quad \dot{e}^{t}_{\theta} = y\dot{\kappa}_{\theta} \tag{4}$$

where $\dot{\kappa}_{r}$ and $\dot{\kappa}_{\theta}$ are curvature rates of the plate defined by the relations

$$\dot{\kappa}_{r} = -\partial\dot{v}/\partial r \quad , \quad \dot{\kappa}_{\theta} = -\dot{v}/r \tag{5}$$

and $\dot{v}$ is the deflection slope rate, i.e.,

$$\dot{v} = \partial\dot{w}/\partial r \, . \tag{6}$$

We denote the intensity rate of the distributed lateral load at a distance r from the center of the plate as $\dot{q}(r,t)$, the shearing force rate per unit length $\dot{Q}(r,t)$ and the bending moment rates per unit length $\dot{M}_{r}(r,t)$ and $\dot{M}_{\theta}(r,t)$ (Fig. 1). Equilibrium requires

$$\partial \dot{M}_r/\partial r + (\dot{M}_r - \dot{M}_\theta)/r + \dot{Q} = 0 \quad \text{and} \tag{7}$$

$$\dot{Q} = \left(\int_0^r 2\pi \dot{q}\xi \, d\xi\right)/(2\pi r) \ , \tag{8}$$

where $$\dot{M}_r = 2\int_0^{h/2} \dot{\sigma}_r y \, dy \quad \text{and} \quad \dot{M}_\theta = 2\int_0^{h/2} \dot{\sigma}_\theta y \, dy \ . \tag{9}$$

In accordance with assumption (iv),

$$\dot{\sigma}_y = 0 \ . \tag{10}$$

The constitutive relations include the generalized Hooke's law and Hart's kinetic equations of creep in terms of a state variable σ^*, called hardness [12],

$$\dot{e}_{ij} = (\dot{\sigma}_{ij} - \nu/(1+\nu)\dot{\sigma}_{\ell\ell}\delta_{ij})/(2G) \tag{11}$$

$$\dot{p} = f(\sigma, \sigma^*, T) \tag{12}$$

$$\dot{\sigma}^* = g(\sigma, \sigma^*, T) \ ,$$

where f and g are experimentally determined functions, σ is the effective stress to be defined later, $\dot{p}$, the effective irrecoverable creep strain rate, T, the temperature, ν, the Poisson's ratio and G, the shear modulus. Following the concepts of incremental plasticity, we define

$$\sigma = ((3/2)s_{ij}s_{ij})^{1/2} \ , \quad \dot{p} = ((2/3)\dot{p}_{ij}\dot{p}_{ij})^{1/2} \tag{13}$$

where

$$s_{ij} = \sigma_{ij} - (1/3)\sigma_{\ell\ell}\delta_{ij} \quad , \tag{14}$$

and the flow rule is given by

$$\dot{p}_{ij} = (3/2)(\dot{p}/\sigma)s_{ij} \quad . \tag{15}$$

In the circular plate, equations (10), (11), (12), (14) and (15) are reduced to:

$$e_r = (\dot{\sigma}_r - \nu\dot{\sigma}_\theta)/E \quad , \quad e_\theta = (\dot{\sigma}_\theta - \nu\dot{\sigma}_r)/E \tag{16}$$

$$\dot{p}_r = (\dot{p}/\sigma)(\sigma_r - \sigma_\theta/2) \quad , \quad \dot{p}_\theta = (\dot{p}/\sigma)(\sigma_\theta - \sigma_r/2) \tag{17}$$

$$\sigma = (\sigma_r^2 + \sigma_\theta^2 - \sigma_r\sigma_\theta)^{1/2} \tag{18}$$

where $E = 2G(1+\nu)$, the Young's modulus.

It must be noted that the constitutive relations are constructed to include classical theories of plasticity which are built upon the concept of a yield function and associated flow rule. Here the strain rate $\dot{p}$ and the hardness rate $\dot{\sigma}^*$ are uniquely defined by the current values of σ, $\dot{\sigma}^*$ and T, independent of the notion of yield stress.

As stated before, the aim here is to obtain a complete set of evolution equations. First we group (3), (4) and (16),

$$\dot{\sigma}_r = -yE(\partial\dot{v}/\partial r + \nu\dot{v}/r)/(1-\nu^2) - E(\dot{p}_r + \nu\dot{p}_\theta)/(1-\nu^2) \quad , \tag{19}$$

$$\dot{\sigma}_\theta = -yE(v/r + \nu\partial\dot{v}/\partial r)/(1-\nu^2) - E(\dot{p}_\theta + \nu\dot{p}_r)/(1-\nu^2) \quad ,$$

and substitute (19) in (9) and integrate,

$$\dot{M}_r = -D(\partial\dot{v}/\partial r+\nu\dot{v}/r) - \Delta\dot{M}_r \quad , \tag{20}$$

$$\dot{M}_\theta = -D(\dot{v}/r+\nu\partial\dot{v}/\partial r) - \Delta\dot{M}_\theta \quad ,$$

where

$$\Delta\dot{M}_r = 2E/(1-\nu^2)\int_o^{h/2}(\dot{p}_r+\nu\dot{p}_\theta)y\,dy \quad , \tag{21}$$

$$\Delta\dot{M}_\theta = 2E/(1-\nu^2)\int_o^{h/2}(\dot{p}_\theta+\nu\dot{p}_r)y\,dy \quad , \text{ and}$$

$$D = Eh^3/(12(1-\nu^2)) \quad . \tag{22}$$

The governing equation is obtained by substituting (20) into the equilibrium equation (7),

$$\partial((1/r)(\partial(rv)/\partial r))/\partial r = \dot{Q}/D - (\partial\Delta\dot{M}_r/\partial r+(\Delta\dot{M}_r-\Delta\dot{M}_\theta)/r)/D \; . \tag{23}$$

Under a set of loading rate conditions, $\dot{Q}$ is given by (8). For the case of constant uniform lateral loading rate $\dot{q}$,

$$\dot{Q} = r\dot{q}/2 \quad , \text{ and} \tag{24}$$

$$\dot{v} = -Ar + Br + \dot{q}r^3/(16D) - \dot{I}/(rD) \quad , \tag{25}$$

where $$I = \left(\int_o^r(\Delta\dot{M}_r-\Delta\dot{M}_\theta)d\xi/\xi\right)(r^2/2) + \left(\int_o^r(\Delta\dot{M}_r+\Delta\dot{M}_\theta)\xi d\xi\right)/2 \quad , \tag{26}$$

and A and B are integration constants to be determined by boundary conditions of a specific problem. The deflection rate $\dot{w}$ is given by (6) together with another boundary condition, whereas the stress rate

and moment rate are made available by inserting (25) into (19) and (20) respectively.

The initial conditions are the solutions of the corresponding elastic plate problem given by any standard text [18], and σ_o^*, initial hardness, is determined experimentally [14].

As the above analysis is quite involved, we will summarize the evolution algorithm:

(i) solve the corresponding elastic plate problem - in particular determine σ_r, σ_θ and v,

(ii) substitute σ_r and σ_θ in (18) to obtain the effective stress which together with σ^* give $\dot{p}$ and $\dot{\sigma}^*$ through Hart's kinetic equations (12),

(iii) $\dot{p}_r$ and $\dot{p}_\theta$ are deduced from the values of $\dot{p}$, σ, σ_r and σ_θ via (17),

(iv) $\Delta\dot{M}_r$ and $\Delta\dot{M}_\theta$ are determined by integrating $\dot{p}_r$ and $\dot{p}_\theta$ according to (21),

(v) $\dot{I}$ is related to $\Delta\dot{M}_r$ and $\Delta\dot{M}_\theta$ as given (26),

(vi) with appropriate boundary conditions $\dot{v}$ given by (25) is solved,

(vii) $\dot{w}$, $\dot{\sigma}_r$, $\dot{\sigma}_\theta$, $\dot{M}_r$ and $\dot{M}_\theta$ are deduced from v through (6), (19) and (20),

(viii) forward integration in time for σ_r, σ_θ, σ^*, v, M_r and M_θ is achieved with any standard routine,

(ix) with new values of σ_r, σ_θ, σ^* and v, steps (ii) through (viii) are repeated.

Euler's method would lead to an increment of deflection slope determined by the relation

$$v|_{t_2} = v|_{t_1} + \dot{v}|_{t_1}(t_2 - t_1) \tag{27}$$

and can provide numerically accurate results as long as Δt is sufficiently small, say $0.1\sigma/\dot{\sigma}$, which has been adequate for the problems discussed here. More refined numerical techniques such as Runge-Kutta or predictor-corrector can be used. The integration is continued until $\dot{\sigma} = \varepsilon$ where ε is a sufficiently small number. It is called the stationary state in the classical creep literature [5].

CIRCULAR PLATE UNDER AXISYMMETRIC LATERAL LOAD

As an example of explicit calculations of deflection, moment and stress, consider a circular plate under constant uniform lateral load q which may subsequently vary with time according to $\dot{q}$. For the sake of definiteness, a well-established form of Hart's law is used [14],

$$\dot{p} = (\sigma^*/D_1)^m(\log(\sigma^*/\sigma))^{-(1/\lambda)}$$

$$\dot{\sigma}^* = \Lambda\dot{p}\sigma^\delta/(\sigma^*)^{\beta-1} \qquad (\dot{}) = \partial()/\partial t \tag{28}$$

where m, λ, δ, β, Λ and D_1 are experimentally determined quantities. D_1 is the only strongly temperature-dependent parameter. Their specific values were given by [14] and [15].

Introduce the following quantities with respect to σ_o which is given later in terms of q, the applied lateral load,

$$v_o = 12\sigma_o a(1-\nu^2)/(Eh) \quad , \quad p_o = \sigma_o(1-\nu^2)/E \quad , \tag{29}$$

$$M_o = \sigma_o h^2 \quad , \quad I_o = \sigma_o a^2 h^2 \quad , \quad D_o = D_1/\sigma_o \quad ,$$

$$t_o = \sigma_o(1-\nu^2)/E(\sigma_o^*/D_1)^{-m}(\log\sigma_o^*/\sigma_o)^{1/\lambda}$$

Note that the above definition of t_o differs from that in the previous report [15] by a factor of $(1-\nu^2)$ which is close to unity for most materials. Therefore the comments made in that report concerning the significance of t_o apply equally well here.

The following dimensionless quantities are defined:

$$\bar{\sigma}_r = \sigma_r/\sigma_o \ , \ \bar{\sigma}_\theta = \sigma_\theta/\sigma_o \ , \ \bar{\sigma}^* = \overset{*}{\sigma}/\sigma_o \ , \tag{30}$$

$$\bar{p}_r = p_r/p_o \ , \ \bar{p}_\theta = p_\theta/p_o \ , \ \bar{\Lambda} = \Lambda\sigma_o^{\delta-\beta+1}(1-\nu^2)/E \ ,$$

$$\bar{v} = v/v_o \ , \ \bar{I} = I/I_o \ , \ \bar{M}_r = M_r/M_o \ ,$$

$$\bar{M}_\theta = M_\theta/M_o \ , \ \overline{\Delta M_r} = \Delta M_r/M_o \ , \ \overline{\Delta M_\theta} = \Delta M_\theta/M_o$$

$$\bar{y} = y/h \ , \ \bar{r} = r/a \ , \ \bar{\xi} = \xi/a$$

$$\bar{t} = t/t_o \qquad (\ )' = \partial(\ )/\partial\bar{t} \ .$$

Henceforth, for simplicity, overbars will no longer be used to denote dimensionless quantities, except where emphasis is necessary.

Two classical problems are examined in detail.

CASE A. Simply Supported Case:

Let $\sigma_o = 3qa^2(3+\nu)//)8h^2)$, the maximum elastic stress. The boundary conditions are,

at $t = 0 \ , \ v(0,0) = M_r(0,1) = 0 \ ,$ (31)

for $t \geq 0 \ , \ v'(t,0) = M_r'(t,1) = 0 \ ,$ and (32)

$$w(t,1) = 0 \ . \tag{33}$$

Following the algorithm stated in the previous section, step (i), i.e.

at $t = 0$,

$$\sigma_r(0,r,y) = 2y(1-r^2) \quad , \quad M_r(0,r) = (1-r^2)/6 \quad ,$$

$$\sigma_\theta(0,r,y) = 2y(1-(1+3\nu)r^2/(3+\nu)) \quad , \quad M_\theta(0,r) = (1-(1+3\nu)r^2/(3+\nu))/6,$$

$$v(0,r) = -r(1/(1+\nu) - r^2/(3+\nu))/6 \quad ,$$

$$\sigma^*(0,r,y) = \sigma_o^* \quad , \quad p_r(0,r,y) = p_\theta(0,r,y) = 0 \quad . \qquad (34)$$

For $t \geq 0$, steps (ii) to (iv) corresponding to (18), (12), (17) and (21),

$$\sigma(t,r,y) = (\sigma_r^2+\sigma_\theta^2-\sigma_r\sigma_\theta)^{1/2} \quad ,$$

$$p'(t,r,y) = (\sigma^*/\sigma_o^*)^m(\log(\sigma^*/\sigma)/\log\sigma_o^*)^{-(1/\lambda)}$$

$$\sigma^{*\prime}(t,r,y) = \Lambda p'\sigma^\delta/(\sigma^*)^{\beta-1}$$

$$p_r'(t,r,y) = p'(\sigma_r-\sigma_\theta/2)/\sigma$$

$$p_\theta'(t,r,y,) = p'(\sigma_\theta-\sigma_r/2)/\sigma$$

$$\Delta M_r'(t,r) = 2\int_o^{1/2} (p_r'+\nu p_\theta')y \, dy$$

$$\Delta M_\theta'(t,r) = 2\int_o^{1/2} (p_\theta'+\nu p_r')y \, dy \quad . \qquad (35)$$

The integrals deduced from (20), (25) and the boundary conditions (32) are defined as follows (steps (v) and (vi))

$$I'_1(r) = \int_0^r (\Delta M'_r - \Delta M'_\theta)d\xi/\xi$$

$$I'_{11} = I'_1(1)$$

$$I'_2(r) = I'_1(r) + \Delta M'_r$$

$$I'_3(r) = r^2 I'_1(r)/2 + \int_0^r (\Delta M'_r + \Delta M'_\theta)\xi d\xi)/2$$

$$I'_{33} = I'_3(1) \quad . \tag{36}$$

Then σ'_r, σ'_θ, v', M'_r and M'_θ are determined; (19) and (20) become

$$\sigma'_r(t,r,y) = 2q'y(1-r^2) + 12y((1-\nu)I'_{33} - I'_{11} - (1-\nu)I'_3/r^2 + I'_2) - (p'_r+\nu p'_\theta)$$

$$\sigma'_\theta(t,r,y) = 2q'y(1-(1+3\nu)r^2/(3+\nu)) + 12y((1-\nu)I'_{33}-I'_{11}+(1-\nu)I'_3/r^2+\nu I'_2)-(p'_\theta+\nu p'_r)$$

$$v'(t,r) = -q'r(1/(1+\nu)-r^2/(3+\nu))/6 + r((1-\nu)I'_{33}-I'_{11})/(1+\nu) - I'_3/r$$

$$M'_r(t,r) = q'(1-r^2)/6 + ((1-\nu)I'_{33}-I'_{11}-(1-\nu)I'_3/r^2+I'_2) - \Delta M'_r$$

$$M'_\theta(t,r) = q'(1-(1+3\nu)r^2/(3+\nu))/6+((1-\nu)I'_{33}-I'_{11}+(1-\nu)I'_3/r^2+\nu I'_2) - \Delta M'_\theta \quad . \tag{37}$$

Finally deflections w are obtained by integrating v with boundary condition (32). For simplicity, all calculations were performed with $q' = 0$, i.e. constant uniform lateral loads only. Fig. 2 shows the deflection profiles of the circular plate at 250°C with two different values of initial hardness, $\bar{\sigma}^*_o$. As intuitively expected, the plate

crept faster in the softer material ($\bar{\sigma}_o^* = 1.5$, upper drawing) than in the harder material ($\bar{\sigma}_o^* = 6.0$, lower drawing) under the same loading. The same conclusion can be drawn by comparing the two deflection profiles of the plate at 22°C are given by Fig. 3. Note the ordinate scale changes for $w/w_o > 1.0$.

The moment distributions of the plate with two values of initial hardness $\bar{\sigma}_o^*$ at 250°C are shown in Fig. 4 which is similar in overall features to that presented by Venkatraman and Hodge in [4]. To gain further insight, stress distributions (these calculations would not be feasible in [4] due to the fact that they used a creep law which is a function of moment multiplied by a function of time) are given by Fig. 5. At $\bar{y} = 0.5$, i.e. the lower face of the plate, both σ_r and σ_θ decreased in magnitude whereas they increased in magnitude at $\bar{y} = 0.1$, near the central plane. That means a more uniform distribution of stress (especially near the center) was attained at stationary state - as expected from past experience. As reported earlier in the creep-bending of beams [15], there was more stress redistribution in the softer material ($\bar{\sigma}_o^* = 0.5$) than in the harder material ($\bar{\sigma}_o^* = 6.0$). The moment distributions at 22°C are shown in Fig. 6.

In all the above cases with initial hardness assumed to be uniform, the change in hardness was less than 1%. However for the case of variable initial hardness, for example, $\bar{\sigma}_o^*(\bar{r},\bar{y}) = \bar{\sigma}_{os}^* \bar{y}$ where $\bar{\sigma}_{os}^*$ is the initial hardness at the surface of the plate, the effect of hardening is evident, as shown in Fig. 7. As $\bar{\sigma}^*$ strongly depends on the relative magnitudes of $\bar{\sigma}^*$ and $\bar{\sigma}$, it is not surprising to observe that hardening is more pronounced near the center where the stress redistribution is the greatest as pointed out before and shown in Fig. 5. Note that the rate of

hardening decreases with time. The effect of initial hardness distribution on deflection is given by Fig. 8 - the deflection with $\bar{\sigma}_o^* = 3\bar{y}$ $(0 < \bar{y} < 0.5)$ is much larger than that with $\bar{\sigma}_o^* = 1.5$, as intuitively expected. Similar remarks on the creep-bending of beams were reported [15].

CASE B. Clamped Case:

Let $\sigma_o = 3qa^2/(4h^2)$, the absolute maximum elastic stress. The boundary conditions are,

$$\text{at } t = 0 \ , \quad v(0,0) = v(0,1) = 0 \ , \tag{38}$$

$$\text{at } t \geq 0 \ , \quad v'(t,0) = v'(t,1) = 0 \ , \text{ and} \tag{39}$$

$$w(t,1) = 0 \ . \tag{40}$$

Again following the algorithm of the previous section, step (i) at $t = 0$,

$$\begin{aligned}
\sigma_r(0,r,y) &= y(1+\nu-r^2(3+\nu)) \ , \\
\sigma_\theta(0,r,y) &= y(1+\nu-r^2(1+3\nu)) \ , \\
v(0,r) &= -r(1-r^2)/12 \ , \\
\sigma^*(0,r,y) &= \sigma_o^* \ , \\
p_r(0,r,y) &= p_\theta(0,r,y) = 0 \ , \\
M_r(0,r) &= (1+\nu-r^2(3+\nu))/12 \ , \\
M_\theta(0,r) &= (1+\nu-r^2(1+3\nu))/12 \ .
\end{aligned} \tag{41}$$

For $t \geq 0$, steps (ii) to (iv) are identical to the expressions given

by (35).

The integrals deduced from (20), (25) and the boundary conditions (39) are also defined according to (36).

Then σ_r', σ_θ', v', M_r' and M_θ' are deduced from (19) and (20),

$$\sigma_r'(t,r,y) = q'y(1+\nu-r^2(3+\nu)) - 12y((1+\nu)I_{33}'+(1-\nu)I_3'/r^2-I_2') - (p_r'+\nu p_\theta')$$

$$\sigma_\theta'(t,r,y) = q'y(1+\nu-r^2(1+3\nu)) - 12y((1+\nu)I_{33}'-(1-\nu)I_3'/r^2-\nu I_2') - (p_\theta'+\nu p_r')$$

$$v'(t,r) = -q'r(1-r^2)/12 + I_{33}'r - I_3'/r$$

$$M_r'(t,r) = q'(1+\nu-r^2(3+\nu))/12 - ((1+\nu)I_{33}' + (1-\nu)I_3'/r^2-I_2') - \Delta M_r'$$

$$M_\theta'(t,r) = q'(1+\nu-r^2(1+3\nu))/12- ((1+\nu)I_{33}' - (1-\nu)I_3'/r^2-\nu I_2') - \Delta M_\theta' \qquad (42)$$

Once again deflections w are obtained by integrating v according to boundary condition (32) and all calculations were performed with $q' = 0$. Fig. 9 shows the deflection profiles of the plate at 250°C with two values of initial hardness $\bar{\sigma}_o^*$. Again creep deformation took place more rapidly in the softer material ($\bar{\sigma}_o^* = 1.5$) than in the harder material ($\bar{\sigma}_o^* = 6.0$). Comparing Fig. 9 in the clamped case with Fig. 2 in the simply supported case, we find that the plate deformed at a slower rate in the former than in the latter as intuitively expected. The deflection profiles at 22°C are given by Fig. 10 and similar conclusions can be drawn.

The moment distributions of the plate at 250°C with two values of initial hardness $\bar{\sigma}_o^*$ are shown in Fig. 11. Note that the stationary state moment distributions are hardly distinquishable from each other. This was also pointed out in [4]. Fig. 12 shows that there was noticeable

difference between the stress distributions corresponding to two values of initial hardness (especially near the center and the edge) although their moment distributions are almost identical. Similar remarks can be made for Fig. 13.

As a final step in analysis, the effect of variable initial hardness distribution is again examined. The growth of hardness of hardness is most pronounced near the edge ($\bar{r} = 1$), quite apparent in the neighborhood of the center ($\bar{r} = 0$), but almost indiscernible in between, as shown in Fig. 14. This correlates well with the intensity of stress redistribution along the radial direction noted earlier. Moreover the maximum change in hardness in this case is less than that in the simply supported case because the stress redistribution is less in the former. The effect on deflection is given by Fig. 15 which is comparable to Fig. 8 with relatively smaller magnitudes (see Fig. 9 versus Fig. 2).

DISCUSSION

Hart's kinetic equations in terms of a state variable called "hardness" have been verified in uniaxial tension for a variety of metals at high temperature [12]-[14]. The extension of this model to the creep-bending of beams has recently been demonstrated by the present authors [15]. Its capability to predict component behavior in a multiaxial state of stress such as creep-bending of plates is, however, not evident. As in the previous report [15], the aim of this paper is twofold: to formulate a technical plate theory, and then to analyze and discuss results obtained by solving practical problems in light of previously published results.

Following the analyses in the previous sections, it was observed that

(i) All the results showed strong influence upon creep deformation of the state variable called "hardness", which is absent in creep theories with time, strain etc. as variables.

(ii) The deflection profiles at 22°C and 250°C in both the simply supported case and the clamped case as given by Figs. 2, 3, 9 and 10 compared qualitatively with figures shown in [4]. Comparing Figs. 2 and 3 with Figs. 9 and 10, we find that the plate deformed at a faster rate in the former than in the latter, as expected.

(iii) The corresponding moment distributions as given by Figs. 4, 6, 11 and 13 also showed features similar to those reported in [4]. It is interesting to note that the stationary state moment distributions for two different values of initial hardness $\bar{\sigma}_o^*$ were essentially indistinquishable in the clamped case.

(iv) The stress distributions in both the simply supported case and the clamped case, not available in the literature, are given by Figs. 5 and 12. Comparing these diagrams with Figs. 4 and 11, we notice

that there were more substantial stress redistributions than corresponding moment redistributions, especially in the neighborhood of the center for both cases and also near the edge for the clamped case. Moreover in the simply supported case, stress decreased in magnitude at the lower face of the plate but increased in magnitude near the central plane, and thus approached a more uniform distribution as intuitively expected.

(v) The choice of time steps was crucial in the numerical analysis using Euler's method. Nonlinear steps (small in the beginning) based on stress redistribution have been employed. A general guide-line is to choose $\Delta\bar{t} < 0.1\ \bar{\sigma}/\bar{\sigma}'$.

(vi) In all the computations with initial hardness assumed to be uniform, the change of hardness was less than 1%. However, with variable initial hardness, e.g. $\bar{\sigma}_o^* = 3\bar{y}(0 < \bar{y} < 0.5)$, the growth of hardness was evident - especially in regions where stress redistributions were most pronounced, as given by Figs. 7 and 14. It is found that hardening rates decreased with time. Moreover the deflections in simply supported and clamped plates shown in Figs. 8 and 15 were less than the corresponding cases with uniform initial hardness $\bar{\sigma}_o^* = 1.5$, as expected.

Note that (i), (v) and (vi) are identical to those stated in the creep-bending of beams [15]. In view of the analyses in the previous sections and the above observations, we believe that the extension of Hart's model to the creep-bending of circular plates which are in a biaxial state of stress has been demonstrated.

As pointed out in [15], a direct constitutive relation between global parameters, i.e., moment, curvature rate and related state-variables will drastically simplify the creep deformation analysis. This will be the subject of a subsequent report.

ACKNOWLEDGEMENTS

This research was supported by Contract No. E(11-1)-2733 of the Energy Research and Development Administration, Washington, D.C. with Cornell University, Ithaca, N.Y. 14853.

REFERENCES

1) Krempl, E., Wells, C.H., and Zudans, Z., "Workshop on inelastic constitutive equations for metals", held July 23-24, 1974 at RPI, supported by NSF, Engineering Division, Solid Mechanics Program.

2) Rabotnov, Y.N., "Creep problems in structural members", North-Holland, Amsterdam (1969).

3) Malinin, N.N., "Continuous creep of round symmetrically loaded plates", (in Russian), Moscow. Vysshee Tekhnicheskoe Uchilishche. Trudy. vol. 26, 221-238 (1953).

4) Venkatraman, B. and Hodge, P.G., Jr., "Creep behavior of circular plates", Jl. Mech. Phys. Solids, 6, 163-176 (1958).

5) Penny, R.K., and Marriot, D.L., "Design for creep", McGraw-Hill, London (1971).

6) Odqvist, F.K.G., "Applicability of elastic analogue in creep problems for plates, membranes and beams", presented at the I.U.T.A.M. colloquium on creep in structures, Stanford Univ., July 11-15, 1960.

7) Patel, S.A., Cozzarelli, F.A., and Venkatraman, B., "Creep of compressible circular plates", Int. Jl. Mech. Sc., 5, 77 (1963).

8) Patel, S.A., "Creep of annular plates under symmetric lateral pressure", Proc. Inst. Mech. Engr. 178 Pt3L, 58-62 (1963-64).

9) Kachanov, L.M., "The theory of creep", National Lending Library for Science and Technology (1967).

10) Sim, R.G., "Creep of structures", Ph.D. dissertation, Univ. of Cambridge (1968).

11) Onat, E.T., and Fardshisheh, F., "Representation of creep of metals", ORNL-4783, Contract #W-7405-eng-26.

12) Hart, E.W., "A phenomenological theory for plastic deformation of polycrystalline metals", Acta Meta, 18, 599-610 (1970).

13) Wire, G.L., Ellis, F.V., and Li, C.-Y., "Work hardening and mechanical equation of state in some metals in monotonic loading", AEC Report #C00-2172-4, Cornell Univ. (1973).

14) Ellis, F.V., Wire, G.L., and Li, C.-Y., "Mechanical properties and mechanical equation of state of 1100 Aluminum alloy in monotonic loading", AEC Report #C00-2172-5, Cornell University (1974).

15) Waung, Y.C., and Lance, R.H., "Creep of beams using a state-variable approach", ERDA Report #C00-2733-6, Cornell University (1976).

16) Kumar, V., and Mukherjee, S., "Creep analysis of structures using new equation of state type constitutive relations", Int. Jl. of Comput. and Struct. (to appear).

17) Nir, N., Hart, E.W., and Li, C.-Y., "An elastic deformation of high purity Aluminum at room temperature", Scripta Meta, 10, 189-194 (1976).

18) Timoshenko, S., and Woinowsky-Krieger, S., "Theory of plates and shells", McGraw-Hill (1959).

FIGURE CAPTIONS

Figure 1 A circular plate under axisymmetric lateral loads

Figure 2 Deflection profile - simply supported
(σ_o = 6.89 MPa (1000 psi), T = 250°C)

Figure 3 Deflection profile - simple supported
(σ_o = 62.05 MPa (9000 psi), T = 22°C)

Figure 4 Moment distribution - simple supported
(σ_o = 6.89 MPa (1000 psi), T = 250°C)

Figure 5 Stress distribution - simply supported
(σ_o = 6.89 MPa (1000 psi), T = 250°C)

Figure 6 Moment distribution - simply supported
(σ_o = 62.05 MPa (9000 psi), T = 22°C)

Figure 7 Growth of Hardness - simply supported

Figure 8 Effect of Initial Hardness Distribution on Deflection - simply supported

Figure 9 Deflection profile - clamped
(σ_o = 6.89 MPa (1000 psi), T = 250°C)

Figure 10 Deflection profile - clamped
(σ_o = 62.05 MPa (9000 psi), T = 22°C)

Figure 11 Moment distribution - clamped
(σ_o = 6.89 MPa (1000 psi), T = 250°C)

Figure 12 Stress distribution - clamped
(σ_o = 6.89 MPa (1000 psi), T = 250°C)

Figure 13 Moment distribution - clamped
(σ_o = 62.05 MPa (9000 psi), T = 22°C)

Figure 14 Growth of Hardness - clamped

Figure 15 Effect of Initial Hardness Distribution on Deflection - clamped

LIST OF SYMBOLS

β Greek lower case beta

δ Greek lower case delta

Δ Greek upper case delta

ϵ Greek lower case epsilon

θ Greek lower case theta

κ Greek lower case kappa

λ Greek lower case lambda

Λ Greek upper case lambda

ν Greek lower case nu

ξ Greek lower case xi

σ Greek lower case sigma

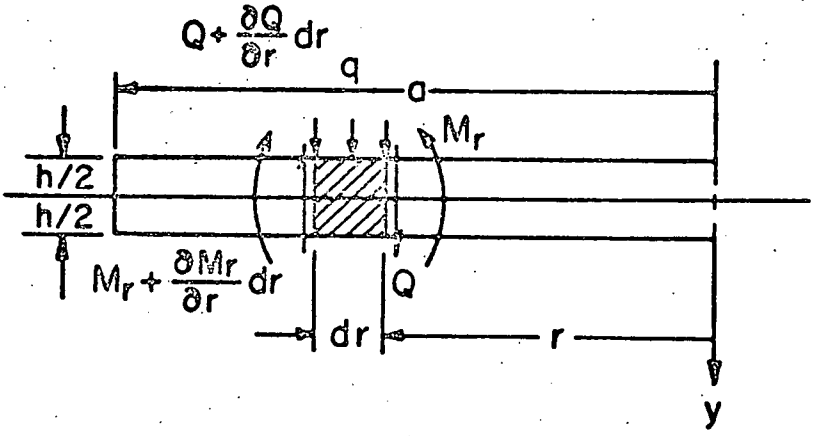
$Q + \frac{\partial Q}{\partial r} dr$
q
a
M_r
h/2
h/2
$M_r + \frac{\partial Mr}{\partial r} dr$
Q
dr
r
y

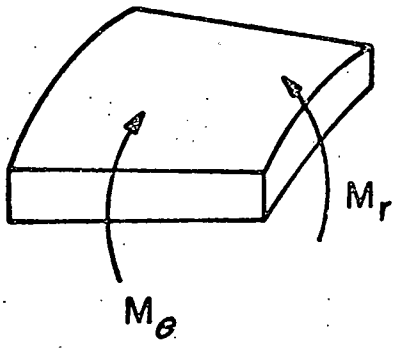
M_r
M_θ

Figure 1.

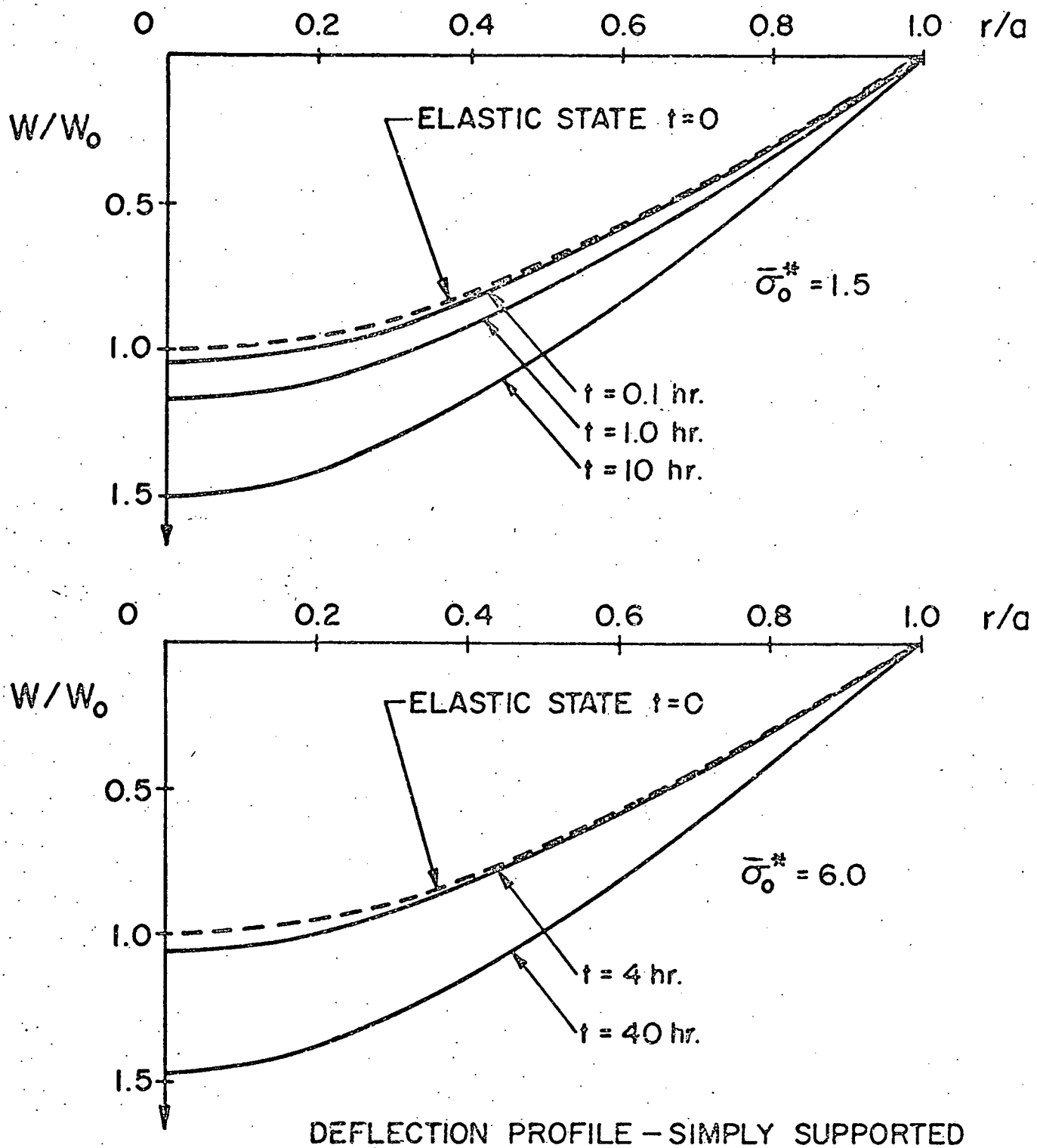

DEFLECTION PROFILE – SIMPLY SUPPORTED

$\sigma_0 = 6.89$ MPa (1000 psi) $T = 250^\circ C$

Figure 2

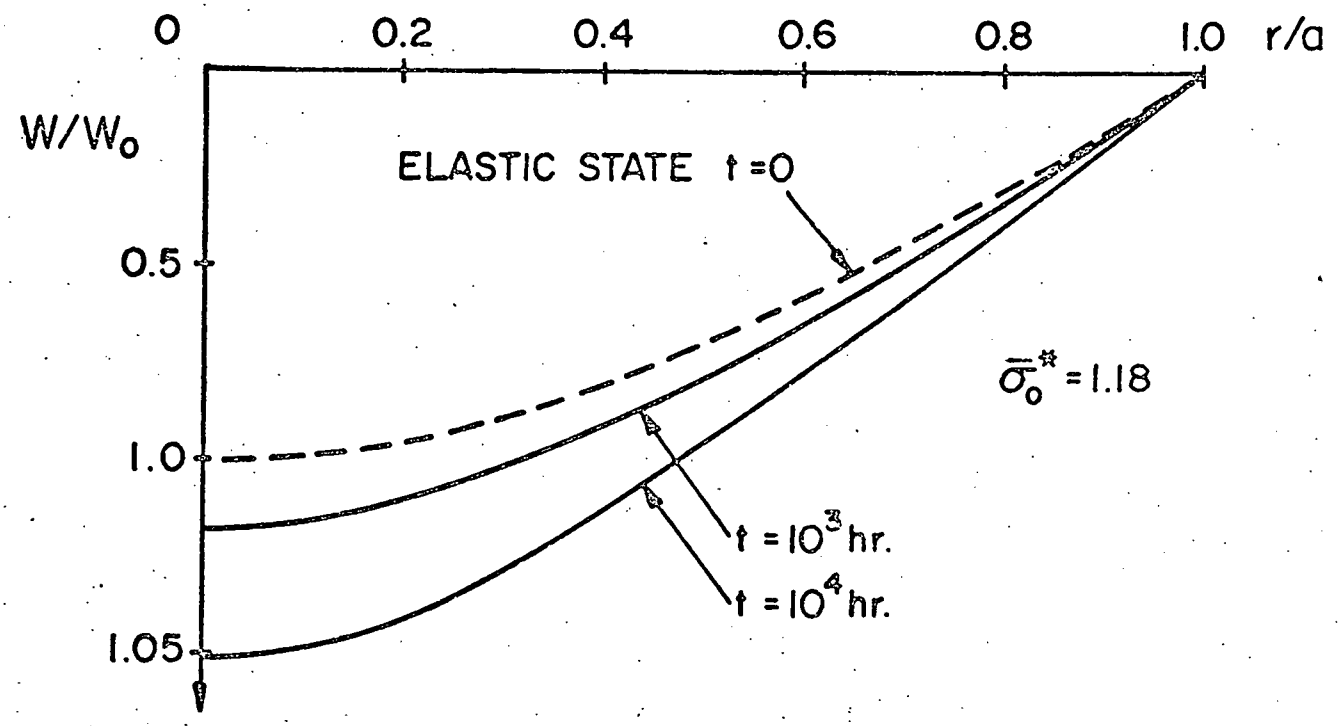

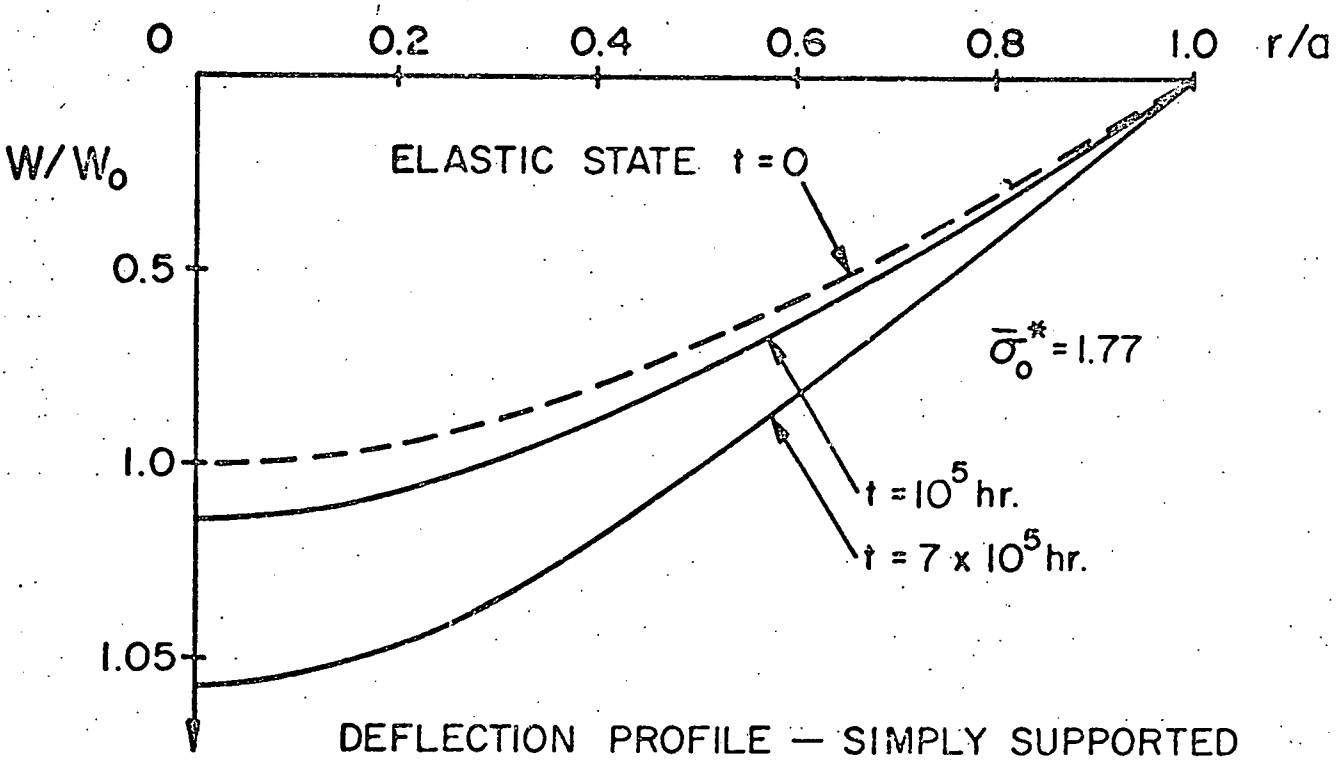

DEFLECTION PROFILE — SIMPLY SUPPORTED

σ_0 = 62.05 MPa (9000 psi) T = 22°C

Figure 3

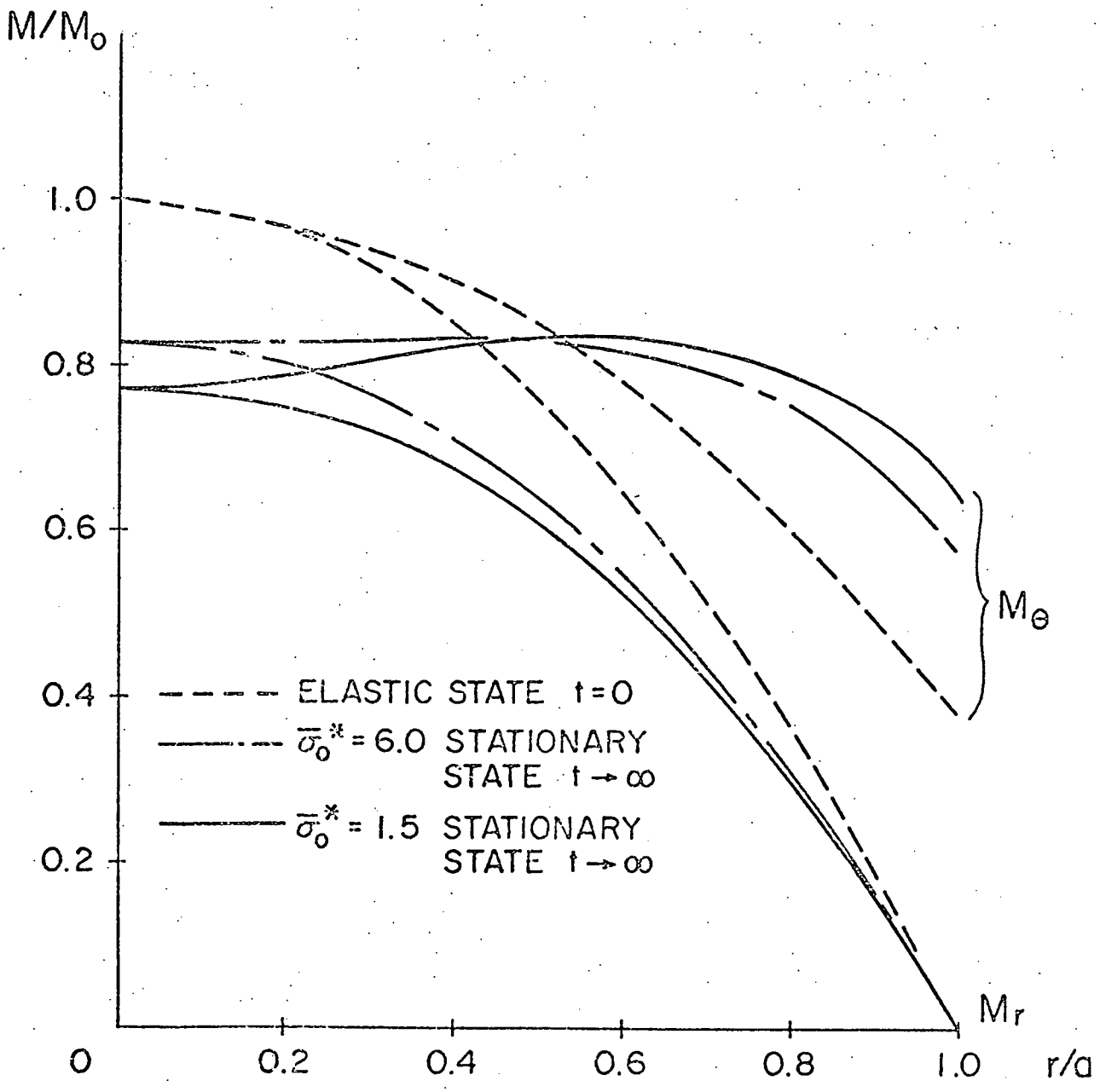

MOMENT DISTRIBUTION – SIMPLY SUPPORTED

σ_0 = 6.89 MPa (1000 psi) T = 250°C

Figure 4

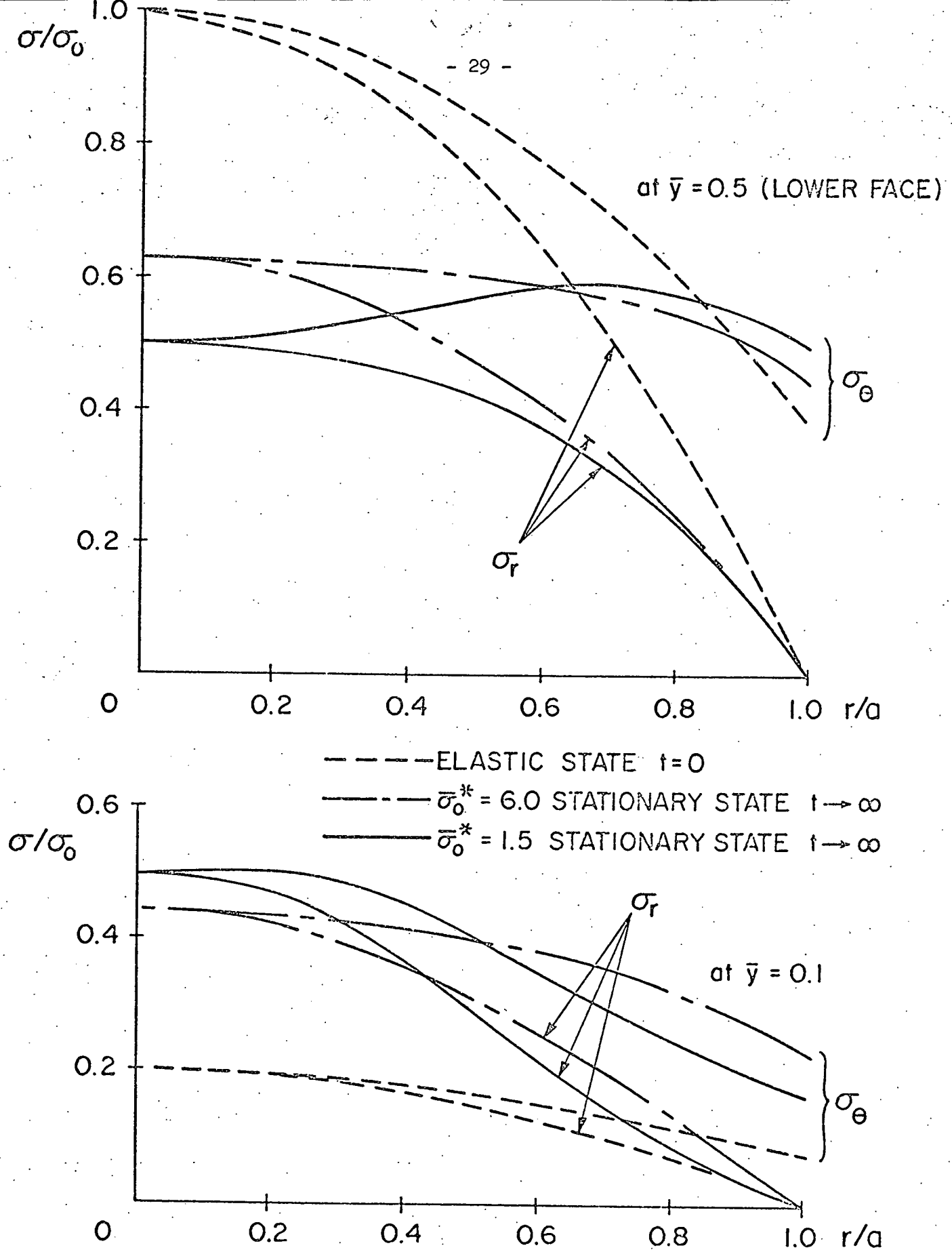

STRESS DISTRIBUTION – SIMPLY SUPPORTED

σ_0 = 6.89 MPa (1000 psi) T = 250°C

Figure 5

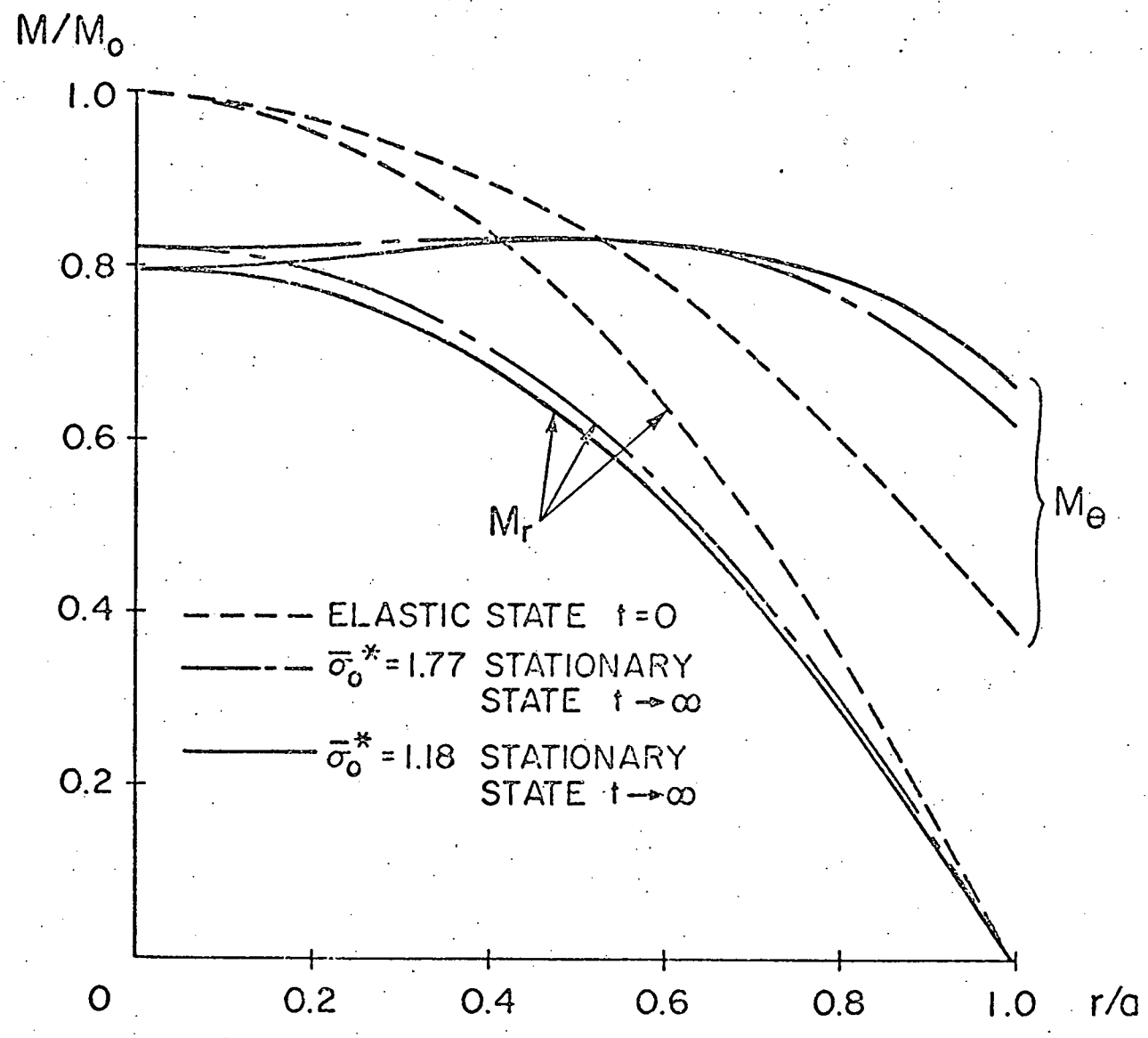

MOMENT DISTRIBUTION – SIMPLY SUPPORTED

σ_0 = 62.05 MPa (9000 psi) T = 22°C

Figure 6

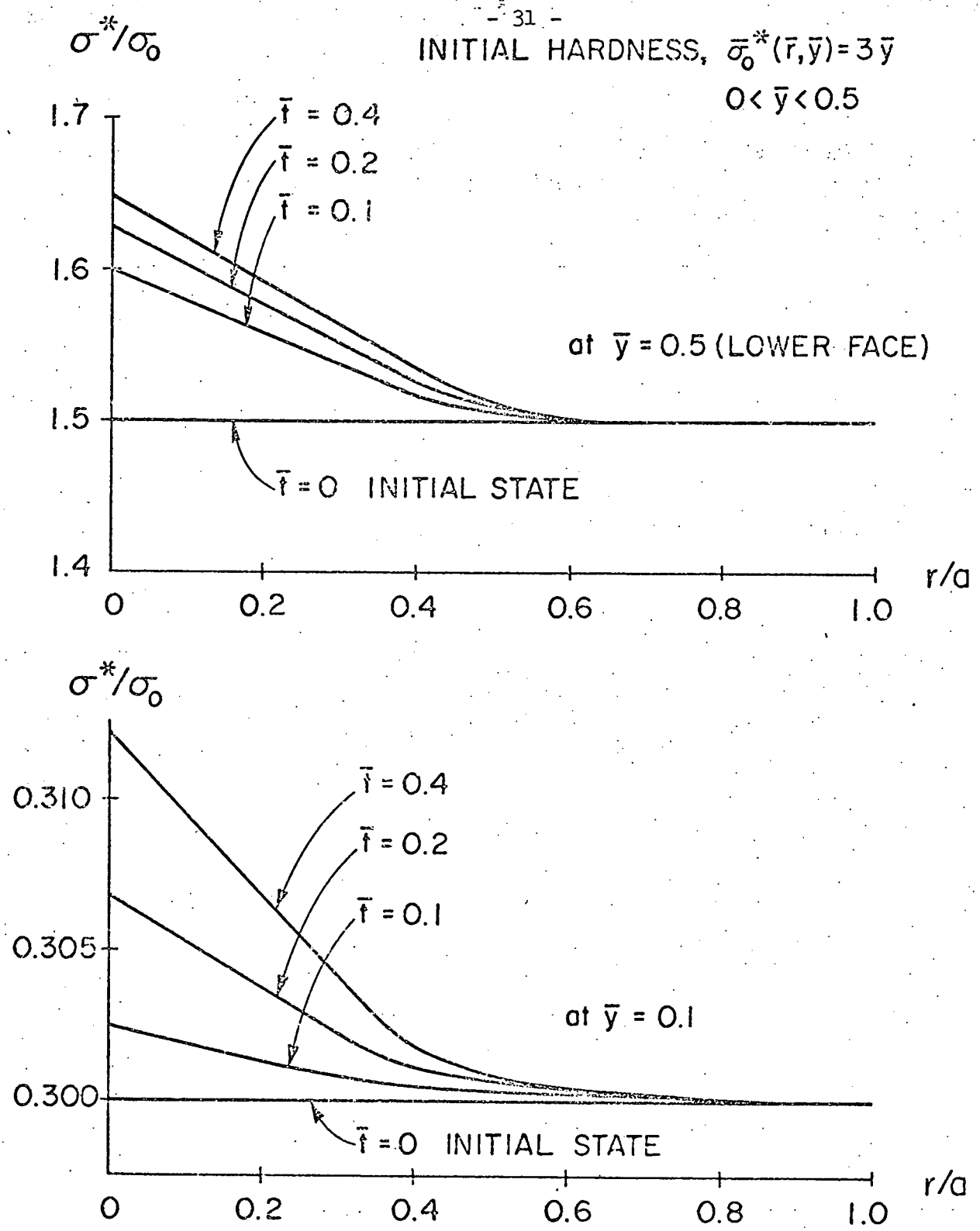

GROWTH OF HARDNESS — SIMPLY SUPPORTED

σ_0 = 6.89 MPa (1000 psi) T = 250°C

Figure 7

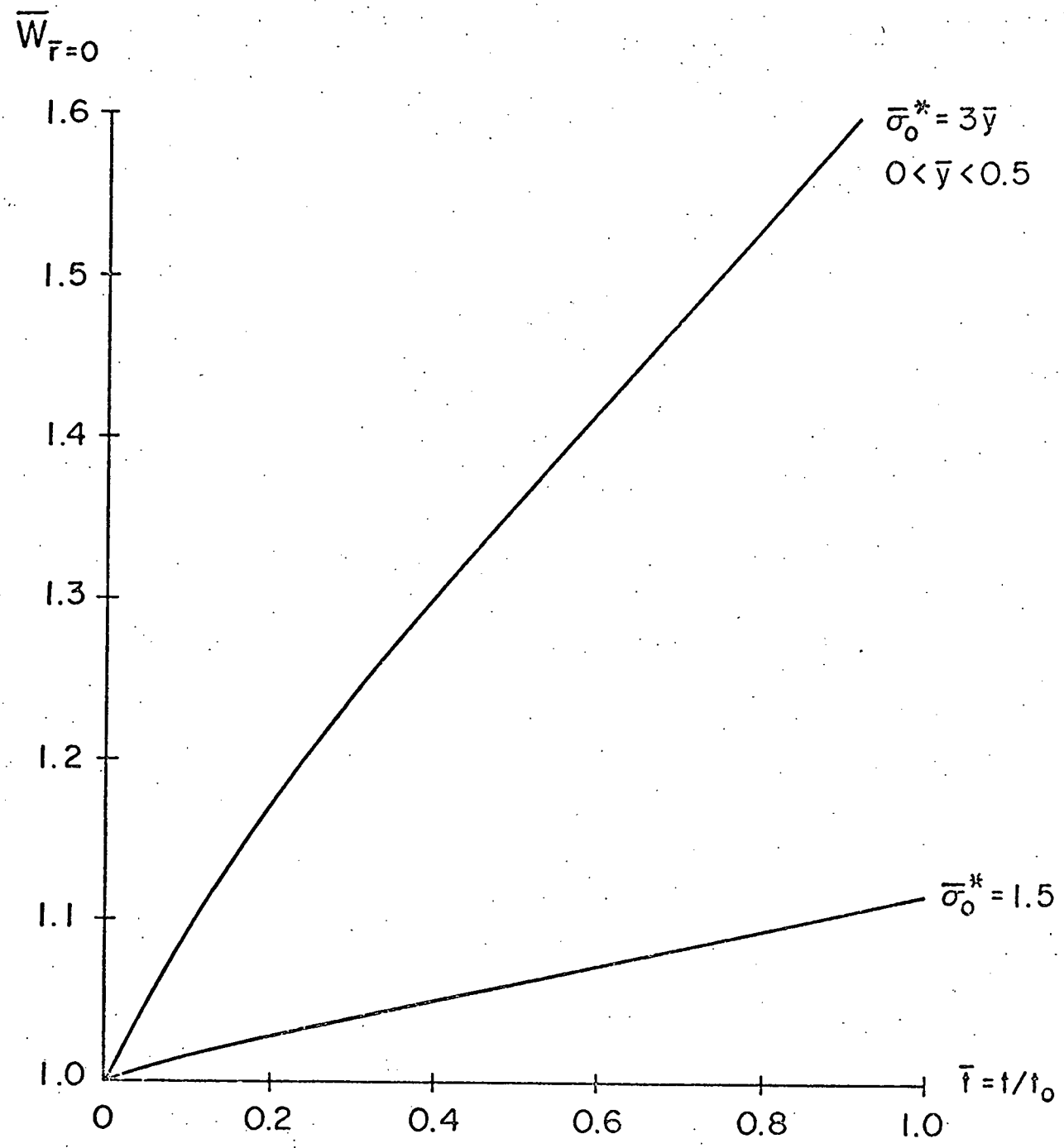

EFFECT OF INITIAL HARDNESS DISTRIBUTION ON DEFLECTION – SIMPLY SUPPORTED

σ_o = 6.89 MPa (1000 psi) T = 250°C

Figure 8

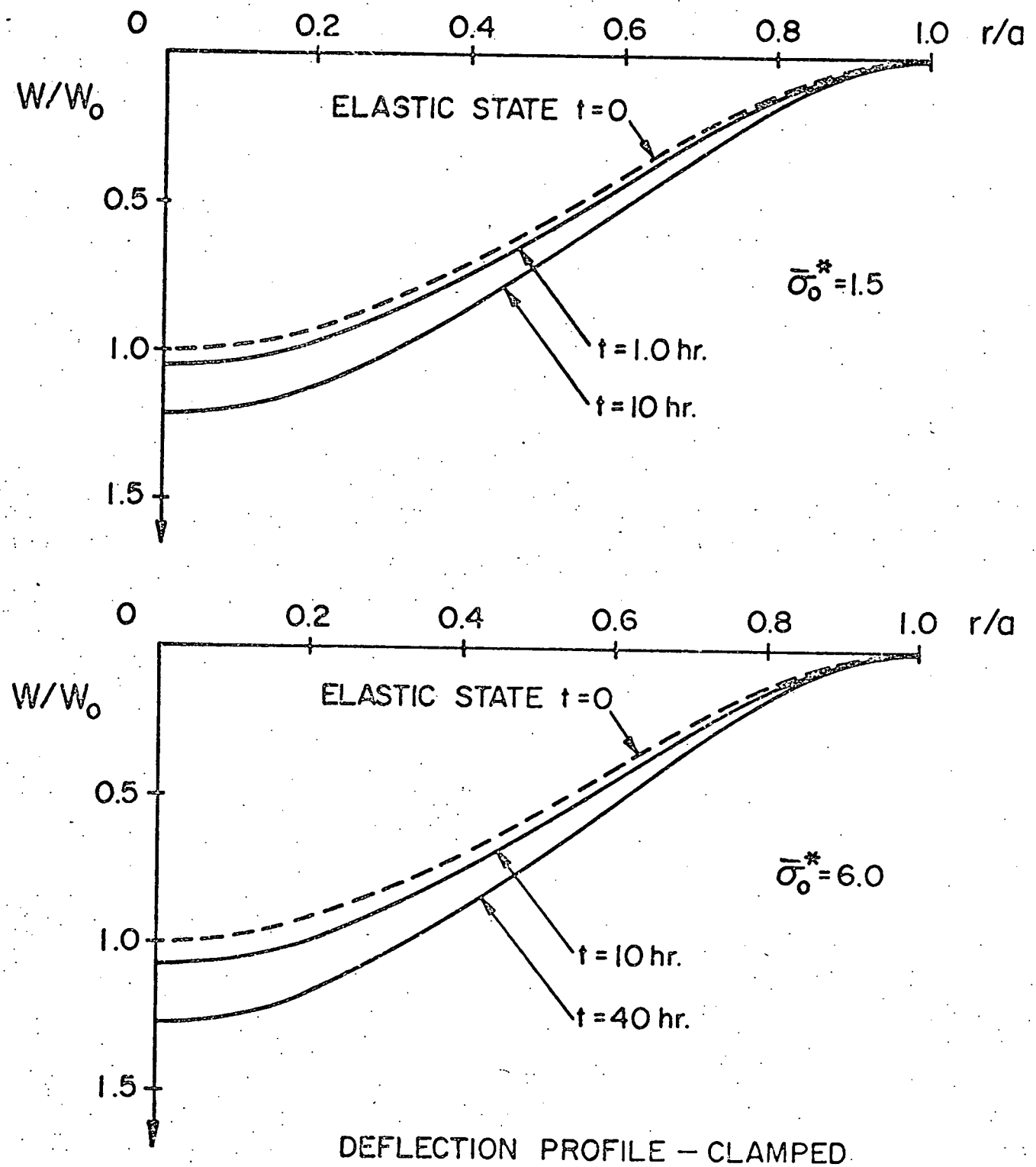

DEFLECTION PROFILE — CLAMPED

σ_0 = 6.89 MPa (1000psi) T=250°C

Figure 9

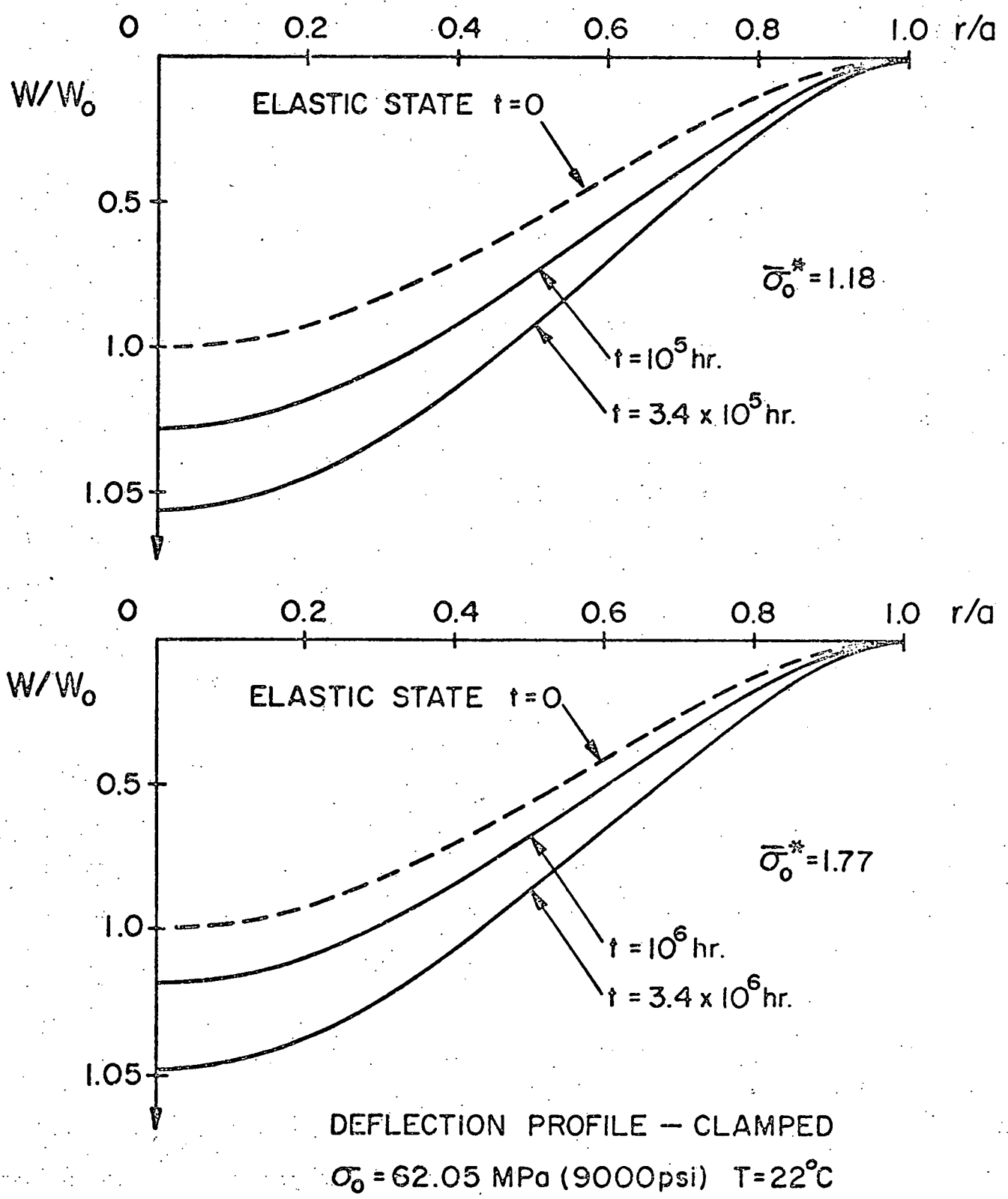

DEFLECTION PROFILE — CLAMPED

σ_0 = 62.05 MPa (9000psi) T=22°C

Figure 10

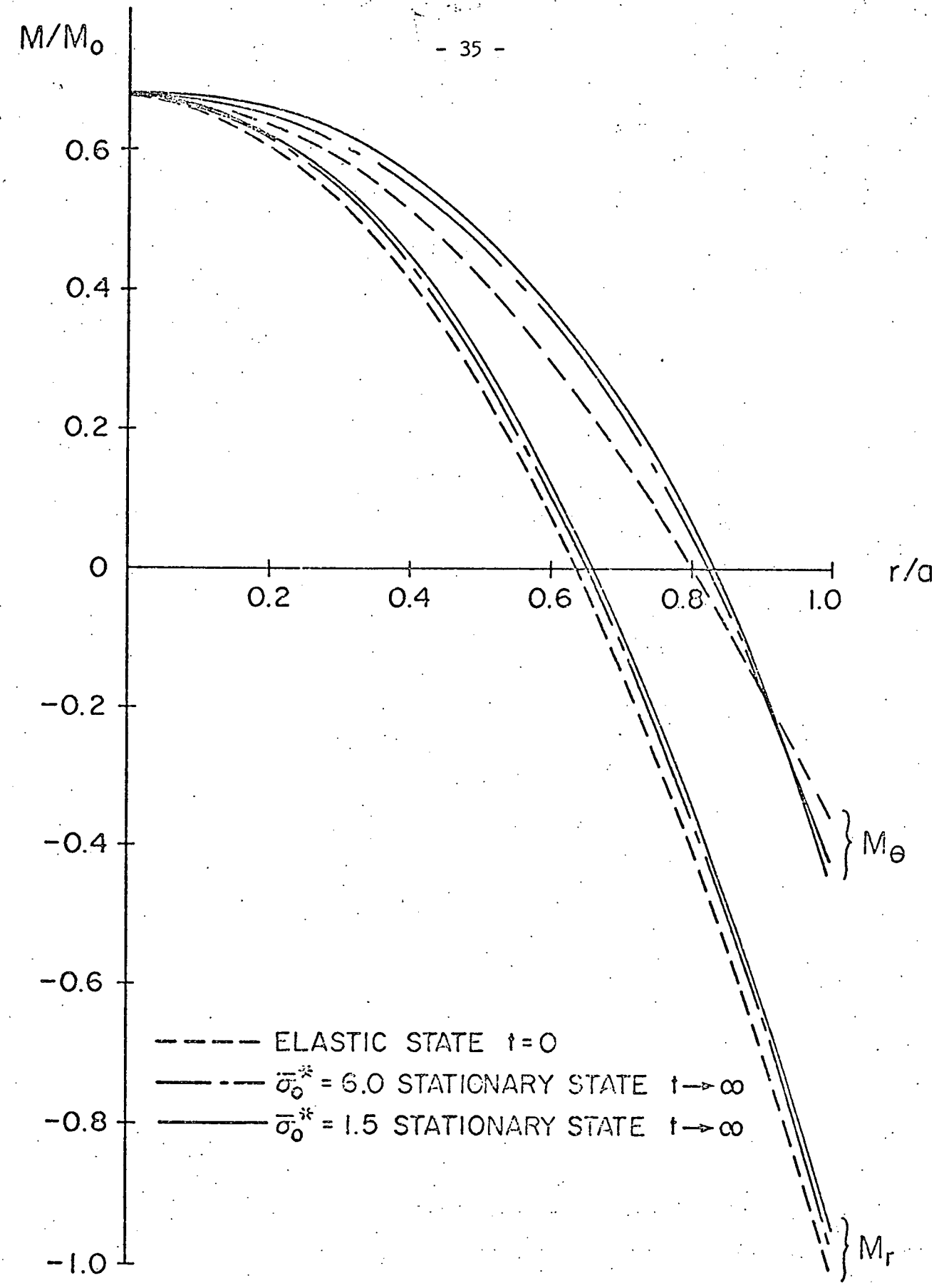

MOMENT DISTRIBUTION — CLAMPED

σ_0 = 6.89 MPa (1000 psi) T = 250°C

Figure 11

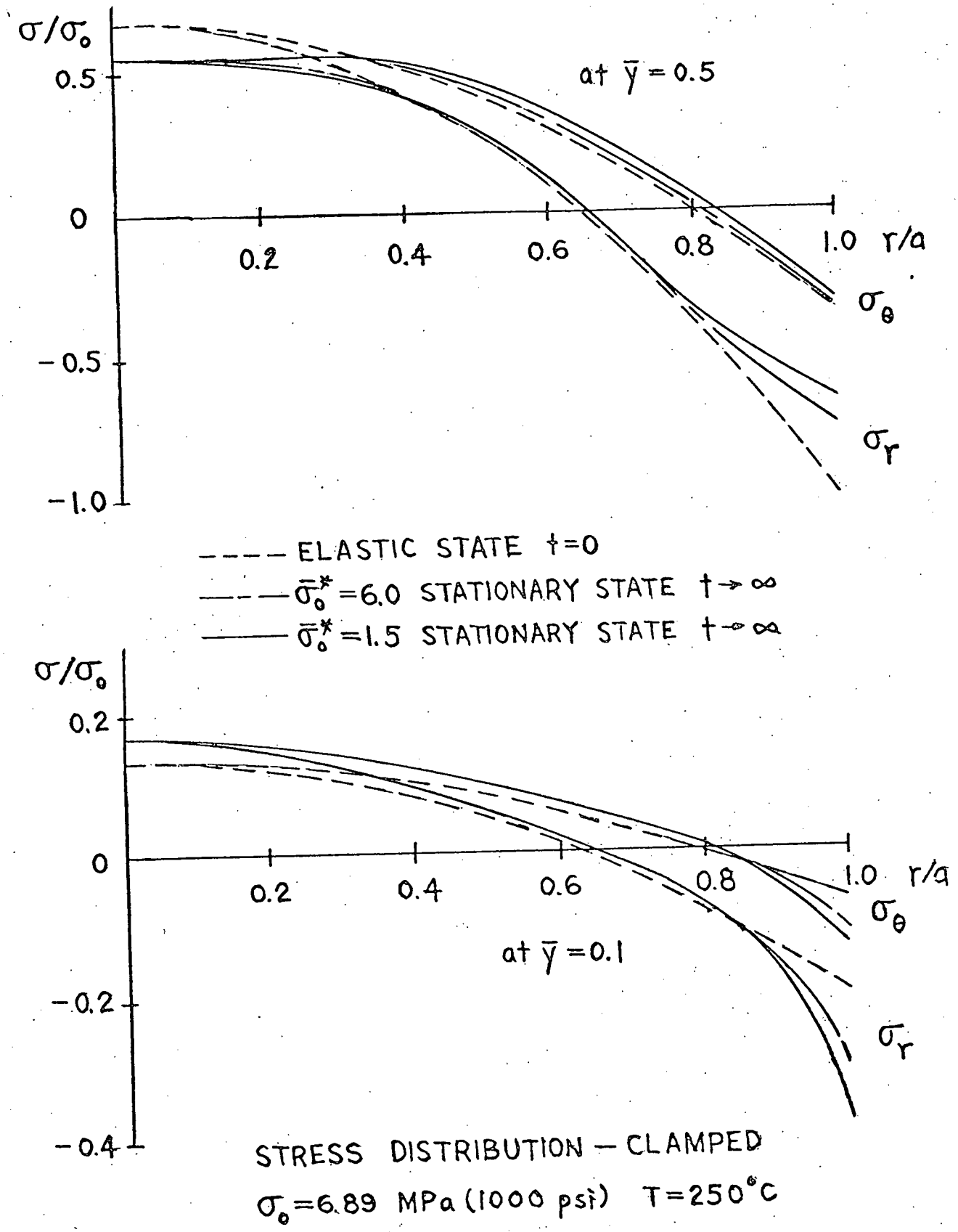
σ/σ₀
0.5
0
-0.5
-1.0
0.2
0.4
0.6
0.8
1.0 r/a
at ȳ = 0.5
σθ
σr
---- ELASTIC STATE t=0
---- σ̄₀* = 6.0 STATIONARY STATE t→∞
—— σ̄₀* = 1.5 STATIONARY STATE t→∞
σ/σ₀
0.2
0
-0.2
-0.4
0.2
0.4
0.6
0.8
1.0 r/a
σθ
at ȳ = 0.1
σr
STRESS DISTRIBUTION — CLAMPED
σ₀ = 6.89 MPa (1000 psi) T = 250°C

Figure 12

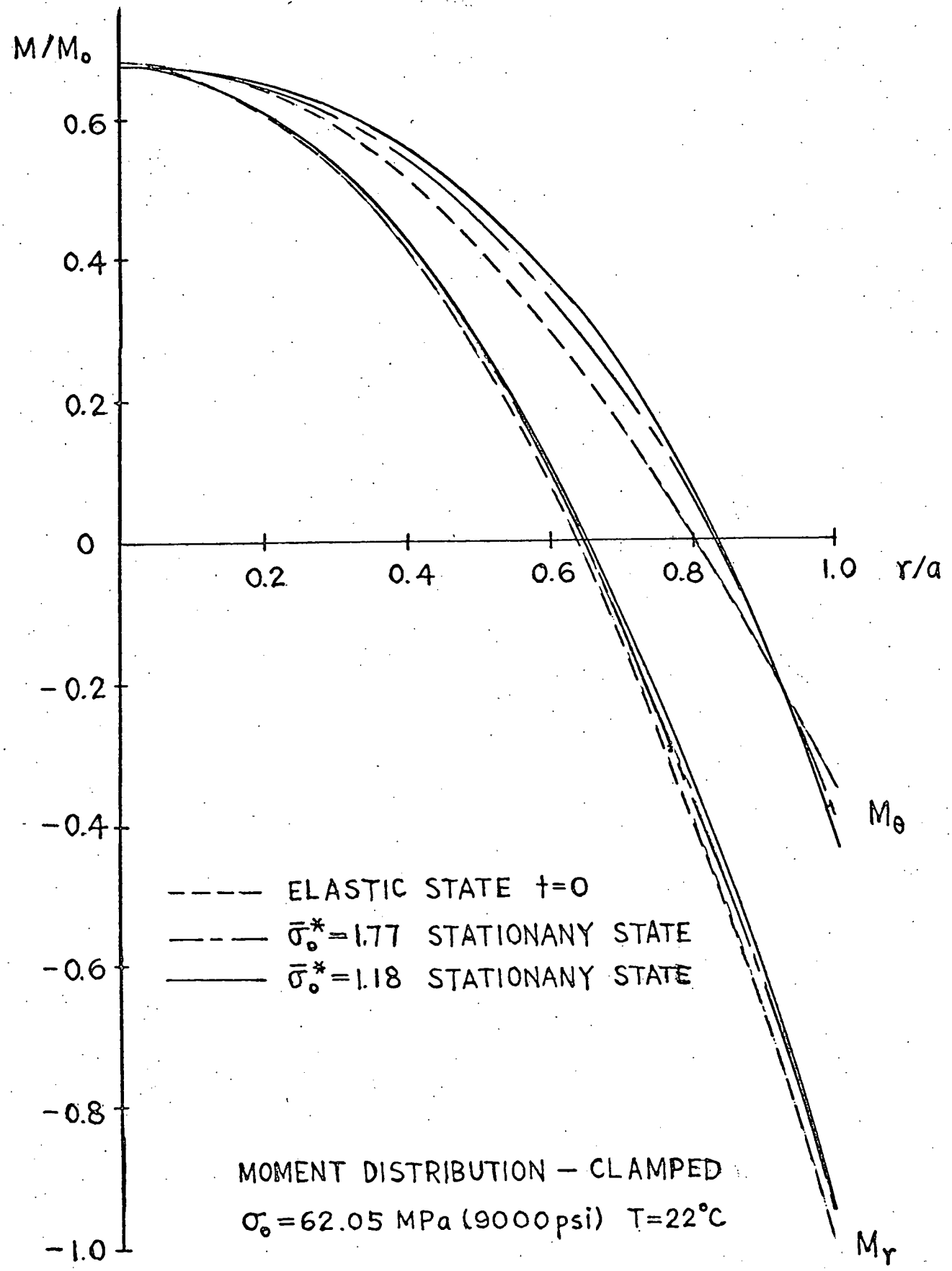
M/M₀
0.6
0.4
0.2
0
-0.2
-0.4
-0.6
-0.8
-1.0
0.2
0.4
0.6
0.8
1.0
r/a
M_θ
M_r
---- ELASTIC STATE t=0
— — — σ̄₀*=1.77 STATIONANY STATE
——— σ̄₀*=1.18 STATIONANY STATE
MOMENT DISTRIBUTION — CLAMPED
σ₀=62.05 MPa (9000 psi) T=22°C

Figure 13

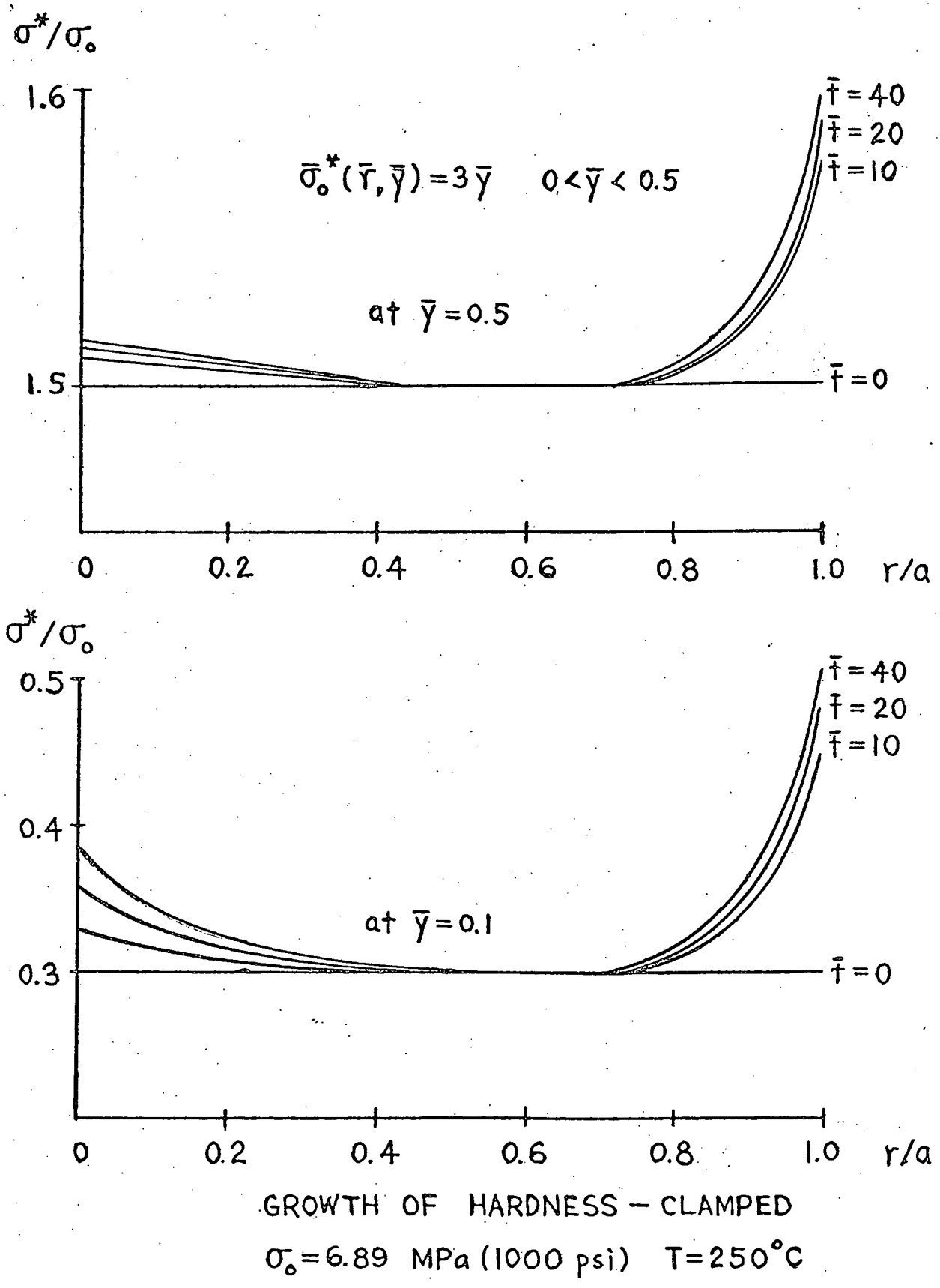
σ*/σ₀
1.6
1.5
$\bar{\sigma}_o^*(\bar{r},\bar{y}) = 3\bar{y}$ $0 < \bar{y} < 0.5$
at $\bar{y} = 0.5$
$\bar{t} = 40$
$\bar{t} = 20$
$\bar{t} = 10$
$\bar{t} = 0$
0
0.2
0.4
0.6
0.8
1.0
r/a
σ*/σ₀
0.5
0.4
0.3
at $\bar{y} = 0.1$
$\bar{t} = 40$
$\bar{t} = 20$
$\bar{t} = 10$
$\bar{t} = 0$
0
0.2
0.4
0.6
0.8
1.0
r/a
GROWTH OF HARDNESS – CLAMPED
σ_o = 6.89 MPa (1000 psi) T = 250°C

Figure 14

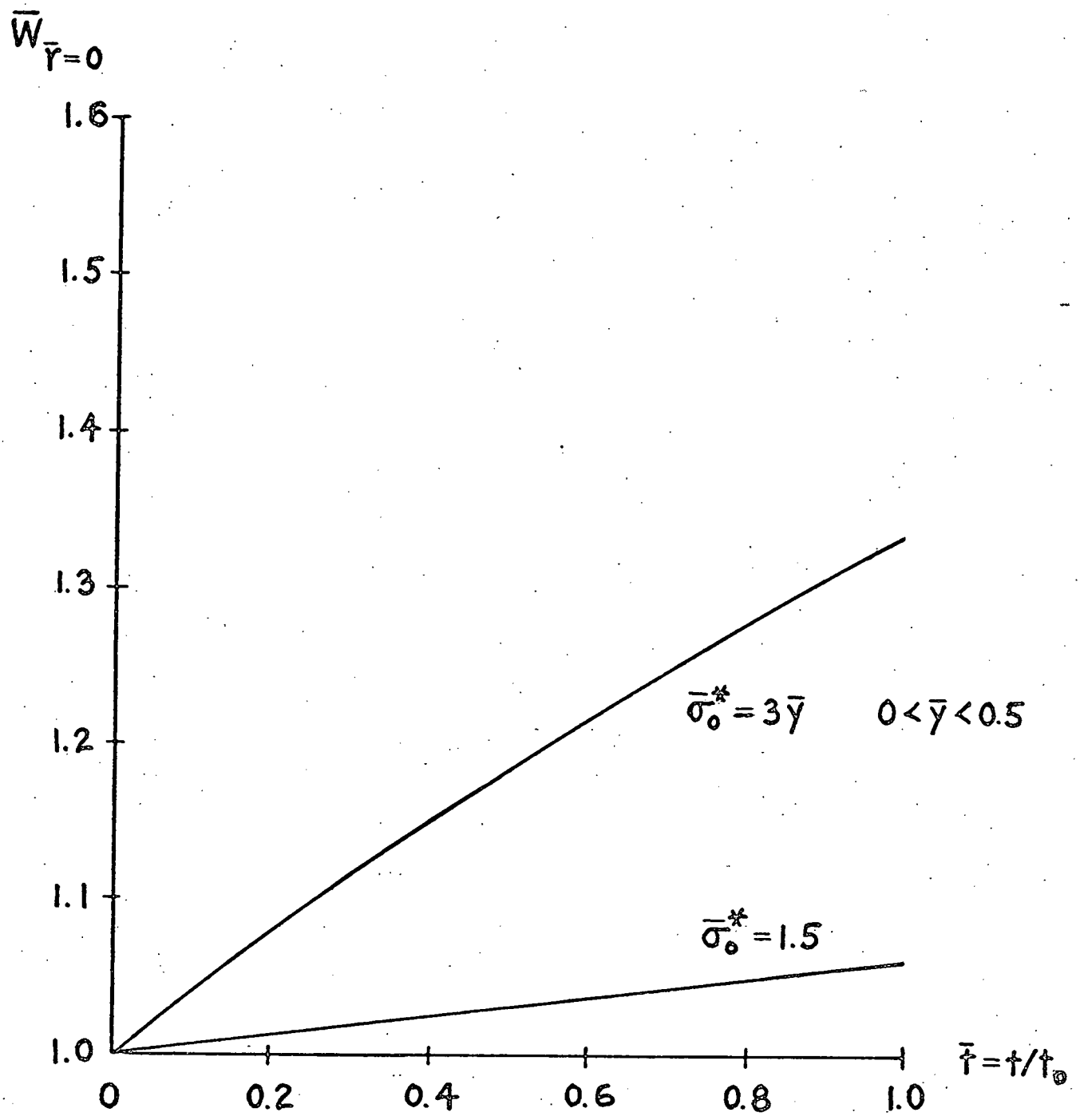

EFFECT OF INITIAL HARDNESS DISTRIBUTION ON DEFLECTION – CLAMPED

$\sigma_o = 6.89$ MPa (1000 psi) $T = 250°C$

Figure 15